Breaking Dynamic Behavior in 3D Covalent Organic Framework with Pre-locked Linker Strategy

Xiaohong Chen , Chengyang Yu , Yusran Yusran , Shilun Qiu , Qianrong Fang *

Posted Date: 27 December 2023

doi: 10.20944/preprints202312.2051.v1

Keywords: covalent organic framework; breaking dynamic behavior; pre-locked linker; gas storage

Article

Breaking Dynamic Behavior in 3D Covalent Organic Framework with Pre-Locked Linker Strategy

Xiaohong Chen [1,‡], Chengyang Yu [2,‡], Yusran Yusran [1,*], Shilun Qiu [1] and Qianrong Fang [1,*]

[1] College of Chemistry, State Key Laboratory of Inorganic Synthesis and Preparative Chemistry, Jilin University, Changchun 130012 P. R. China

[2] College of Chemistry and Environmental Engineering, Wuhan Polytechnic University, Wuhan 430023, P. R. China

* Correspondence: authors: postys@jlu.edu.cn (Y. Y.); qrfang@jlu.edu.cn (Q. F.)

‡ These authors contributed equally.

Abstract: As for their large surface area and pore volume, three-dimensional covalent organic frameworks (3D COFs) have emerged as competitive porous materials. However, due to the structural dynamic behavior particularly for imine-linked 3D COFs, potentially unlock their potential for gas storage application. Herein, we showed a pre-locked linker strategy introduces breaking dynamic behavior in 3D COFs. A predesigned planar linker based 3,8-diamino-6-phenylphenanthridine (DPP) was prepared to produce non-dynamic 3D JUC-595, as benzylideneamine moiety in DPP locked the linker flexibility and restrict the molecular-bond rotation of the imine linkages. Upon solvent inclusion and release, the PXRD profile of JUC-595 remained intake, while JUC-594 with flexible benzidine linker experienced crystal transformation due to framework contraction-expansion. As a result, the activated JUC-595 achieved higher surface areas (754 $m^2 g^{-1}$) than that of JUC-594 (548 $m^2 g^{-1}$). Furthermore, improved CO_2 and CH_4 storages were also seen in JUC-595 compared with JUC-594. Impressively, JUC-595 recorded high normalized H_2 storage capacity that surpass other reported high surface area 3D COFs. This works shows important insight on manipulating structural properties of 3D COF to tune the gas storage performance.

Keywords: covalent organic framework; breaking dynamic behavior; pre-locked linker; gas storage

1. Introduction

Covalent organic frameworks (COFs) are constructed by predesigned organic molecules linked through covalent bonds into two and three-dimensional (2D/3D) networks[1–10]. Compared to 2D COFs, 3D COFs are far excellent for gas storages due to their high surface areas and capable to load more active sorption sites[11–15]. However, structural dynamic behavior in 3D COFs as inexistence of interlayer π-π bonding could greatly hinder the gas adsorption and storage capabilities of this material. Specifically, it propagates structural expansion and contraction upon guest absorption, release and exchanges[16]. Crucially, this structural transformation often reduces the surface areas, pore size as well as pore volume, thereby reducing the gas storage capacity. For instance, LZU-301 governed by flexible imine linkages and bipyridine linker experienced framework contraction after guest removal, causing significant Brauner-Emmett-Teller surface areas (SA_{BET}) reduction from 848 $m^2 g^{-1}$ to 654 $m^2 g^{-1}$[17]. Meanwhile, imine-linked 3D-CageCOF-1 which constituted by a flexible cage-like triangular prism knot exhibited reversible pore structure switching from large-pore (lp) to small-pore (sp) architectures after the trapped DMF molecules were removed within the pores[18]. Breaking dynamic behavior in 3D COFs is thus pivotal to tackles such structural deformation disadvantage, aiming to achieve high surface areas 3D COFs that close to its theoretical values as well as to improve the gas storage performances.

Current strategy for breaking dynamic behavior in 3D COFs was by constructing supramolecular forces within the established 3D framework such as steric hindrance and H-bonding

 doi:10.20944/preprints202312.2051.v1

to restrict the molecular bond rotation and contraction of the skeleton[19,20]. In this regard, we have reported the design and synthesis of two non-dynamic 3D COFs (JUC-552 and JUC-570) by rationally designing linkers containing alkyls groups as side chains to promote steric hindrance[21,22]. The skeleton of JUC-552 remained less-flexible or rigid as the presence of crowded four symmetric methyl groups restricted the molecular bond rotation of imine linkages, affording an exceptional SA_{BET} (up to 3023 $m^2 g^{-1}$) compared with that non-functionalized 3D COF analogue (JUC-550, SA_{BET} = 846 $m^2 g^{-1}$)[21]. Likewise, steric hindrance caused by the isopropyl groups in JUC-570 kept the imine linkages to be less-rotatable, thus lead to a nearly 4-folds increase in SA_{BET} relative to unfunctionalized 3D COF analogue (JUC-571)[22]. Meanwhile, the dynamic behavior of dynaCOF-301 was significantly altered as the presence of hydroxyl (–OH) groups near the imine linkages evolved H-bonding, enforcing the framework upon removal and inclusion of guest molecule[23]. Although these strategies obviously restrict or breaking the dynamic behavior in 3D COFs, specific design of building units and precise synthetic condition need to be considered to evolve such supramolecular bonds within framework. Therefore, exploration new and simpler strategy to tackle the structural dynamic issues in 3D COFs is emergent yet challenging.

Herein, we report a novel yet simple strategy for breaking dynamic behavior in 3D COFs by the use of pre-designed conformationally-locked linker (Scheme 1a). Detailly, pre-locked linker-based 3,8-diamino-6-phenylphenanthridine (DPP) was chosen to condense with a tetrahedral knot-based tetrakis-(4-formylphenyl)adamantane (TFPA) to afford non-dynamic JUC-595 as the benzylideneamine moiety in DPP locked the linker flexibility and thus restrict the molecular-bond rotation of the imine linkages in JUC-595. For a comparison, TFPA was further condensed with a flexible linker-based benzidine (BD) to produce dynamic JUC-594. JUC-594 experienced reversible crystal phase transformation upon solvent inclusion and release as the impact of framework contraction-expansion, while JUC-595 show PXRD profile unchanged confirming the breaking dynamic behavior. Hence, the activated JUC-595 exhibited higher SA_{BET} and pore volume than that of JUC-594, manifesting the firm of framework upon activation. Accordingly, JUC-595 documented higher CO_2 and CH_4 storages compared with JUC-594. Furthermore, JUC-595 recorded notable normalized H_2 storage capacity surpassing other reported high surface area 3D COFs. This works demonstrated facile textural property tuning in 3D COFs and paves the development of functional 3D COFs for gas storage application.

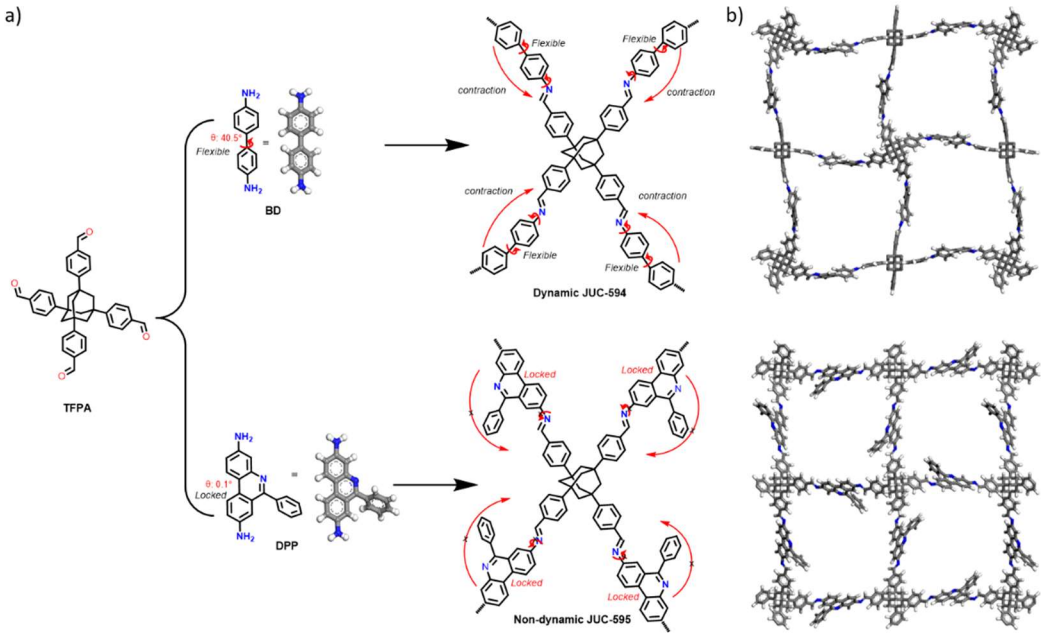

Scheme 1. Rational design of non-dynamic 3D COFs via locked linker strategy. Design JUC-594 and JUC-595. a) Design and synthesis of dynamic JUC-594 and non-dynamic JUC-595 employing flexible BD and planar DPP linkers. b) The 3D representative crystal models of JUC-594 (top) and JUC-594 (down) with 2-fold **dia** net viewed along c axis.

 doi:10.20944/preprints202312.2051.v1

2. Materials and Methods

2.1. Materials

Unless specified otherwise, all initial materials and solvents were purchased from J&K Scientific LTD. Reagents and solvents are in high purity and used upon received without additional purification.

2.2. Synthesis of dynamic JUC-594

JUC-594 has been prepared elsewhere (termed as DbTd) but with very poor crystallinity[24], thus it may be considered as amorphous polymer. JUC-595 in this work, was prepared in different condition to obtain highly crystalline 3D COF. Specifically, TFPA (0.025 mmol, 13.8 mg) and BD (0.050 mmol, 9.2 mg) were placed into a Pyrex glass tube. Subsequently, 1,4-dioxane (0.75 mL), mesitylene (0.25 mL) and aqueous acetic acid (6 M, 0.1 mL) were added. The tube was flash-frozen in a liquid nitrogen bath and the internal pressure was maintained at 19.0 mbar under vacuum. It was then sealed by flame and reduced length by *ca.* about 12.0 cm before being placed in an oven at 120 °C for three days to afford a yellow crystalline powder. It was then washed with acetone for 5 times and immersed in hexane. Activation was performed by vacuum drying at 20 mTorr under 65 °C. Anal. Cald: C: 86.86; H: 5.14; N: 8.00. Found: C: 86.56; H: 5.27; N: 8.17.

2.3. Synthesis of non-dynamic JUC-595

TFPA (0.020 mmol, 11.0 mg) and DPP (0.040 mmol11.4 mg) were placed into a Pyrex tube. Subsequently, mesitylene (1 mL) and 6 M aqueous acetic acid (6 M, 0.1 mL) were added into tube. The tube was flash-frozen in a liquid nitrogen bath and the internal pressure was maintained at 19.0 mbar under vacuum. Upon warming to room temperature, the tube was placed in an oven at 120 °C for three days. The resultant precipitate was filtered and washed with acetone for 5 times. It was then immersed in hexane. Activation was performed by vacuum drying at 20 mTorr under 65 °C. Anal. Cald: C: 88.57; H: 4.76; N: 6.67. Found: C: 88.30; H: 4.91; N: 6.79.

2.4. Characterization

The Fourier transform infrared spectrophotometer (FT-IR) were obtained using a SHIMADZU IRAffinity-1. Thermogravimetric analysis (TGA) was recorded on a SHIMADZU DTG-60 thermal analyzer under N_2 at 30 °C to 800 °C with heating rate of 10 °C min^{-1}. The powder X-ray diffraction (PXRD) data were collected on a PANalytical B.V. Empyrean powder diffractometer using a Cu Kα source (λ = 1.5418 Å) over the range of 2θ = 2.0-40.0° with a step size of 0.02° and 2 s per step. The sorption isotherms for N_2, CH_4, CO_2 and H_2 were measured using a Quantachrome Autosorb-IQ analyzer with ultra-high-purity gas (99.999 % purity). Before gas adsorption measurements, the as-synthesized COFs (~50.0 mg) were immersed in acetone for 12 h (5 × 20.0 mL) and then n-hexane for another 12 h (5 × 10.0 mL). The n-hexane was then extracted under vacuum at 65 °C to afford the samples for sorption analysis. To estimate pore size distributions for both JUC-594 and JUC-595, nonlocal density functional theory (NLDFT) was applied to analyze the N_2 isotherm on the basis of the model of N_2@77K on carbon with slit pores. The electron microscopy (SEM) images were acquired using JEOL JSM-6700 SEM. Meanwhile, the transmission electron microscopy (TEM) images were taken with JEOL JEM2100F.

3. Results and Discussion

3.1. Design and synthesis of dynamic JUC-594 and non-dynamic JUC-595

The grand design on breaking dynamic behavior in 3D COFs in this work was to condense a locked biphenyl linker (DPP) to afford a rigid and non-flexible 3D framework (JUC-595, Scheme 1). Contrast phenomenon was expected for 3D COF with flexible BD linker (JUC-594), prompting reversible framework expansion-contraction driven by rotatable imine bond upon guest removal and

 doi:10.20944/preprints202312.2051.v1

inclusion[25]. In practical, both JUC-594 and JUC-595 were synthesized via acid-catalyzed Schiff-based solvothermal condensation among TFPA with either DPP or BD at 120 °C for 3 days.

The FT-IR spectra of both 3D COFs exhibit a stretching band at 1625 and 1626 cm^{-1} for JUC-594 and JUC-595 respectively, indicating the evolution of C=N bonds. Additionally, the absence of N-H stretching vibration signal from BD (3321≈3208 cm^{-1}) and DPP (3328≈3212 cm^{-1}) as well as the significant diminishment of the C=O vibration signal of TFPA (1695 cm^{-1}), further confirmed the successful of Schiff-base condensation reaction (Figure S1 and S2). Meanwhile, the morphology of both COF observed under SEM and TEM analysis revealed that both COFs crystallized into a homogeneous rod-like crystals (Figures S3 and S4). Furthermore, TGA analysis confirmed that both COFs are thermally stable up to 450 °C under N_2 atmosphere (Figures S5 and S6).

The crystallinity and unit cell parameters of both COFs were resolved by PXRD analysis in conjunction with structural simulations using Materials Studio software package (Figure 1)[26]. The crystal model of both JUC-594 and JUC-595 adopted a 2-fold interpenetrated **dia** net with corresponding cell parameters of a = b = 42.2408 Å, c = 31.5544 Å, and $\alpha = \beta = \gamma = 90°$ for JUC-594 and a = b = 44.7519 Å, c = 27.9163 Å, and $\alpha = \beta = \gamma = 90°$ for JUC-595 (Scheme 1b). The experimental PXRD profile the fresh JUC-594 exhibits intense peaks at 4.04 and 4.66°, as well as several moderate peaks at 6.52, and 9.40°, corresponding to the (111), (210), (221), and (322) Bragg peaks of P-4B2 space group (Figure 1). Following the same space group, the intense PXRD peaks for JUC-595 are observed at 3.91 and 4.38° with moderate peaks at .92, 7.80, and 9.51° belonging to the (200), (210), (112), (321), and (003) Bragg peaks. Full-profile pattern matching (Pawley) refinements were performed based on the experimental and simulated data, revealing a good agreement factors (R_p = 3.81%; R_{wp} = 5.05 % for JUC-594 and R_p = 0.91%; R_{wp} = 1.37% for JUC-595). Alternative structures such as non-interpenetrated or multi-fold interpenetrated **dia** nets were also considered, but the simulated PXRD profiles were inconsistent with the experimental ones (Figures S7 and S8). Based on these results, it is proposed that both 3D COFs adopt 2-fold interpenetrated **dia** net.

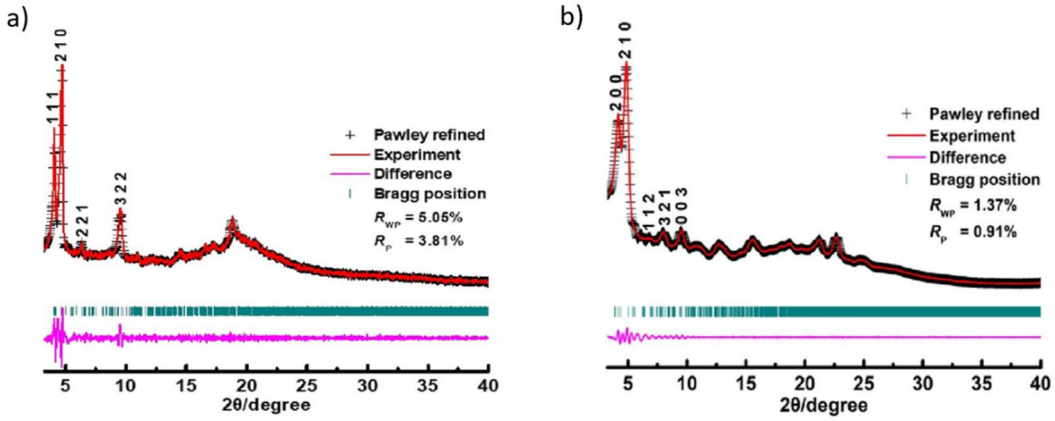

Figure 1. The simulated and experimental PXRD patterns of a) JUC-594 and b) JUC-595.

3.2. Structural dynamic behavior of JUC-594 and JUC-595

It has been observed that dynamic behavior of porous materials could induce reversible crystal transition due to the framework contraction-expansion caused by guest molecule, pressure, or temperature [17,27–29]. In this work, we propose pre-locked linker strategy to breaking dynamic behavior in 3D COF. Firstly, the PXRD profiles of both COFs under solvated (hexane) and activated conditions were recorded (Figures S9 and S10). Obviously, JUC-594 shows PXRD profile discrepancy among the solvated and activated samples meaning that both samples have a different crystal phase (Figure S9). Meanwhile, the PXRD profiles of JUC-595 depict similarity for both solvated and activated conditions, confirming that the inclusion and exclusion of solvent do not affect the framework (Figure S10). To get insight into this guest molecule-triggered crystal transition, PXRD profiles of both COFs upon evaporating the trapped hexane at different times were further recorded to observe their structural dynamic responsivity (Figure 2). Apparently, the peaks at 2θ = 4.66 and 4.04° of solvated JUC-594 were gradually merged into an intense peak at 4.07° upon gradually

Preprints (www.preprints.org) | NOT PEER-REVIEWED | Posted: 27 December 2023 doi:10.20944/preprints202312.2051.v1

evaporating hexane in the pores within 1–20 minutes in room temperature (Figure 2a). This quick PXRD peak change identifies the structural dynamic behavior responsive in JUC-594, leading to the framework unit cell expansion along the *a*- and *b*-axes upon guest molecule release. Interestingly, the former two peaks re-split upon resoaked into hexane confirming the framework contracted upon solvation. Hence, JUC-594 show reversible structural dynamic behavior. Unlike framework contraction upon activation found in dynamic FCOF-5 and LZU-301 with non-bulk tetraphenylmethane knot[17,28], we assumed that the presence of hydrophobic hexane molecule in JUC-549 may attract pore surface procuring framework contraction. More importantly, the bulkier of TFPM knot may causes less-dynamic character in JUC-594 compared with FCOF-5 and LZU-301.

In contrast, PXRD profiles of JUC-595 remained unchanged upon hexane inclusion and release from the pores (Figure 2b). This observation indicates that JUC-595 does not undergo crystal transformation caused by hexane molecules as the framework remains rigid and flexible. As we proposed, the intramolecular locking by benzylideneamine moieties in DPP could cause molecular bond-rotation restriction on imine linkages, breaking the dynamic behavior in JUC-595.

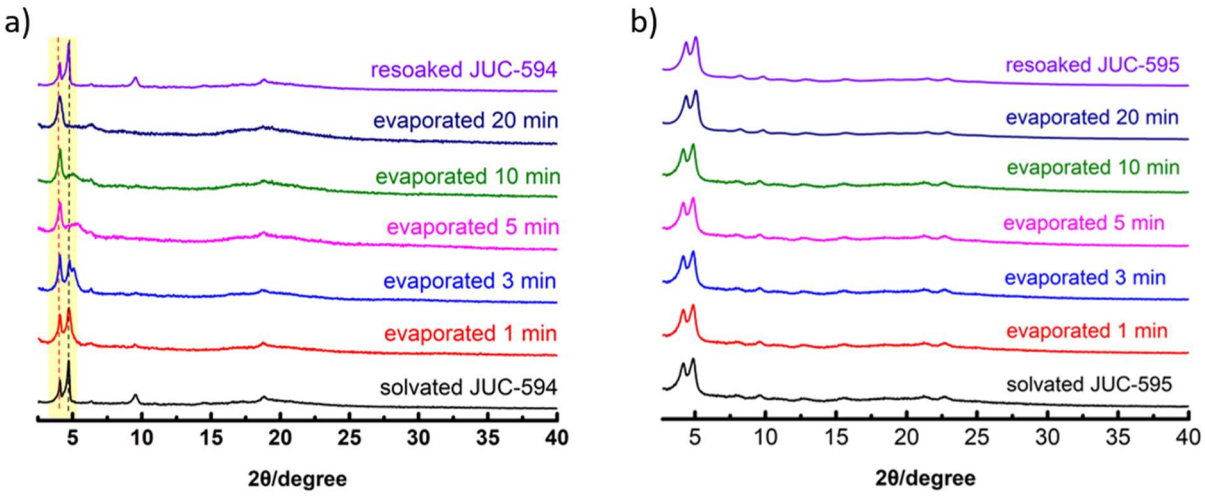

Figure 2. PXRD profiles of solvated (hexane) a) JUC-594 and b) JUC-595 upon evaporating hexane molecule in room temperature.

Structural dynamic in 3D COFs greatly affect the pore character, thus determine the surface areas and pore volume. In this regard, N_2 adsorption-desorption analyzes were conducted at 77 K to evaluate the permanent porosity of both 3D COFs (Figure 3 and S11–S13). Both COFs exhibited type-I isotherms with a sharp uptake observed below $P/P_0 = 0.05$, characteristics of microporous materials (Figure 3a). Comparatively, based on these isotherms the activated JUC-595 recorded a higher Brunauer–Emmett–Teller specific surface areas (BET SSA) (754 $m^2\ g^{-1}$) in comparison with the activated JUC-594 (548 $m^2\ g^{-1}$) (Figure S11 and S12). The lower SSA of JUC-594 may attribute to the framework contraction upon activation due to its structural dynamic behavior. Additionally, the N_2 adsorption isotherm feature of JUC-594 displays an obvious hysteresis loop, indicating structural dynamic response upon N_2 molecules release from the pore (Figure S13)[17]. Furthermore, both COFs showed a distinct pore size distributions calculated by nonlocal density functional theory (NLDFT) method (Figure 3b-c). JUC-594 afforded a dominant pore size of about 1.09 nm with a pore volume of 0.247 $cm^3\ g^{-1}$, narrower than that of JUC-595 (dominant pore size = 1.46 nm, pore volume = 0.553 $cm^3\ g^{-1}$). Meanwhile, the predicted pore size of simulated non-contracted JUC-594 is wider (2.2 nm) than that of obtained from experimental result, revealing the N_2 molecule-triggered pore change (Figure S14). In contrast, JUC-595 confirmed comparable pore size among the experimental and simulated non-contracted framework (1.6 nm), strengthening the non-dynamic framework upon guest molecule inclusion-exclusion (Figure 15).

Preprints (www.preprints.org) | NOT PEER-REVIEWED | Posted: 27 December 2023 doi:10.20944/preprints202312.2051.v1

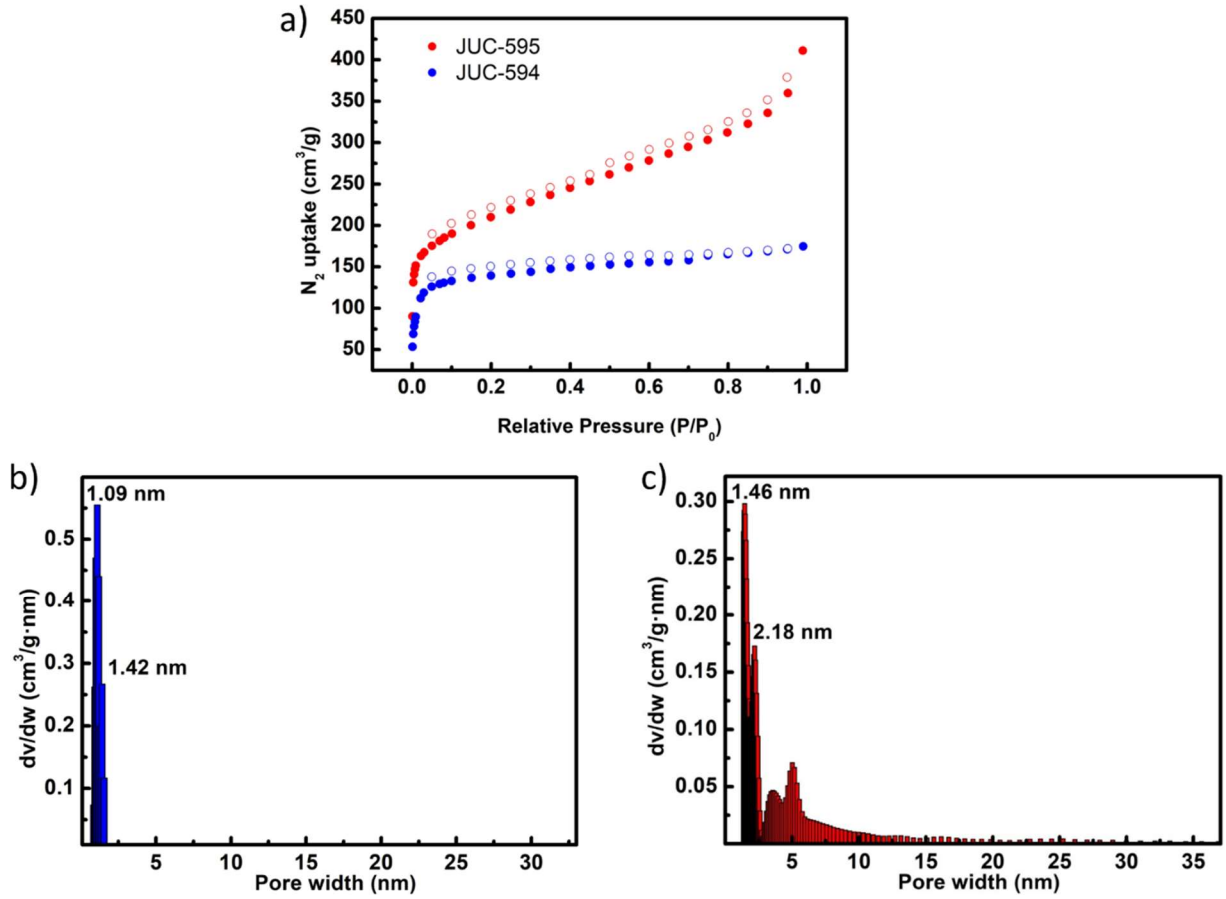

Figure 3. Porosity analysis of JUC-594 and JUC-595. a) N_2 adsorption-desorption isotherm comparison of JUC-594 and JUC-595. Pore size distribution of b) JUC-594 and c) JUC-595 calculated by NLDFT method.

3.2. Gas storage performance of JUC-594 and JUC-595

Having observed that tuning the structural dynamic affects the porosity of both 3D COFs, we then sought to study their CO_2, CH_4, and H_2 storage performances. In pursuit, the CO_2 and CH_4 gases storages of JUC-594 and JUC-595at 273 and 298K were firstly compiled as these gases possess a comparable molecular size (Figure 4). At lower temperature (273K), JUC-594 recorded a CO_2 adsorption capacity as high as 34 $cm^3\ g^{-1}$ and experienced storage declined down to 22 $cm^3\ g^{-1}$ at 298 K (Figure 4a-b). Comparatively, JUC-595 exhibited higher adsorption capacities at similar conditions (44 and 30 $cm^3\ g^{-1}$ at 273 and 298 K, respectively). Similar trends were observed for CH_4 as gas probe, in which JUC-595 stored as high as 11 $cm^3\ g^{-1}$ of the gas at 273 K and 7 $cm^3\ g^{-1}$ at 298 K, slightly surpassing the performance of JUC-594 (9 and 5 $cm^3\ g^{-1}$ at 273 and 298 K, respectively) (Figure 4c-d). We assumed that the increased adsorption capacities of JUC-595 compared with JUC-594 for both gas probes correlates to their distinct porosity characters as the impacts of their dissimilar structural dynamic behavior.

Preprints (www.preprints.org) | NOT PEER-REVIEWED | Posted: 27 December 2023 doi:10.20944/preprints202312.2051.v1

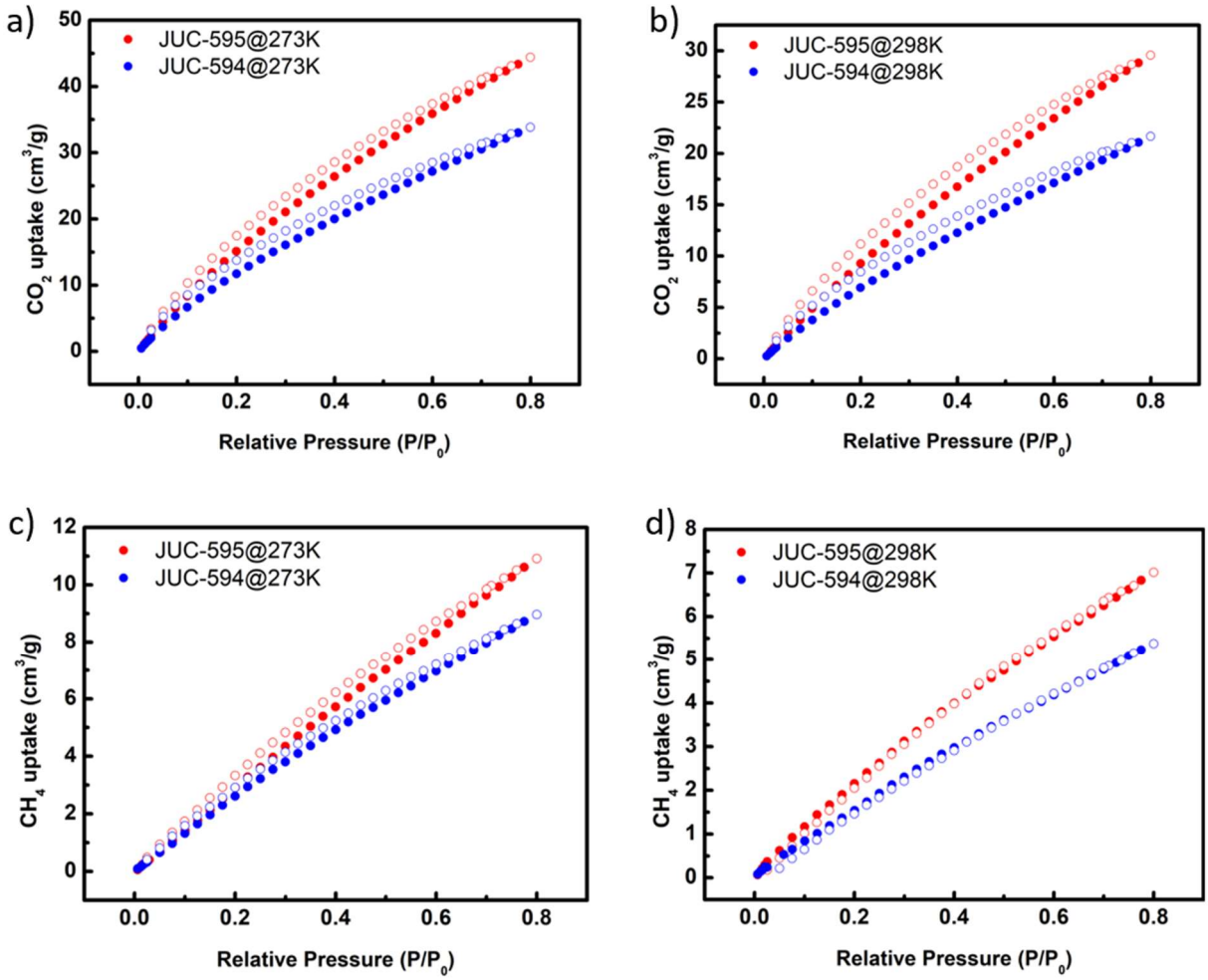

Figure 4. CO_2 adsorption isotherms for a) JUC-594, b) JUC-595 and CH_4 adsorption isotherms for c) JUC-594, d) JUC-595.

Considering the highly valuable and renewable of H_2 as cost-effective fuels alternative to fossil fuel in the future[30], the potential H_2 storage of JUC-594 and JUC-595 was further investigated. In particular, JUC-594 exhibited H_2 adsorption capacity as high as 55 $cm^3\ g^{-1}$ at 77 K and 38 $cm^3\ g^{-1}$ at 87 K (Figure 5a). Notably, JUC-595 reached an H_2 adsorption capacity of 96 cm^3/g^{-1} at 77 K and 65 $cm^3\ g^{-1}$ at 87 K, which are nearly double than that of JUC-594 under identical test conditions (Figure 5b). To gain a better understanding on the improved H_2 storage in JUC-595, the H_2 isosteric heat adsorption (Q_{st}) was calculated based on the H_2 adsorption tests at different temperatures. Apparently, the calculated Q_{st} for JUC-595 was about 6.57 kJ mol^{-1}, higher than that of JUC-594 (5.36 kJ mol^{-1}) (Figure S14 and S15). These findings suggest that the interaction H_2 with JUC-595 is stronger compared with JUC-594. The enhanced sorbate sorbent interaction in JUC-595 is likely attributed to the presence of more adsorption active sites as well as the non-dynamic frameworks maintained the surface area and pore volume. More importantly, the surface area normalized H_2 sorption capacity of JUC-595 at 77 K (0.13 $cm^3\ m^{-2}$) is far superior in comparison with other reported 3D COFs, including COF-103(0.04 $cm^3\ m^{-2}$)[31], JUC-596 (0.12 $cm^3\ m^{-2}$)[32], JUC-597 (0.08 $cm^3\ m^{-2}$)[32], and comparable with that of highly-connected 3D JUC-568 (0.19 $cm^3\ m^{-2}$)[33] at similar condition (Table S1).

 doi:10.20944/preprints202312.2051.v1

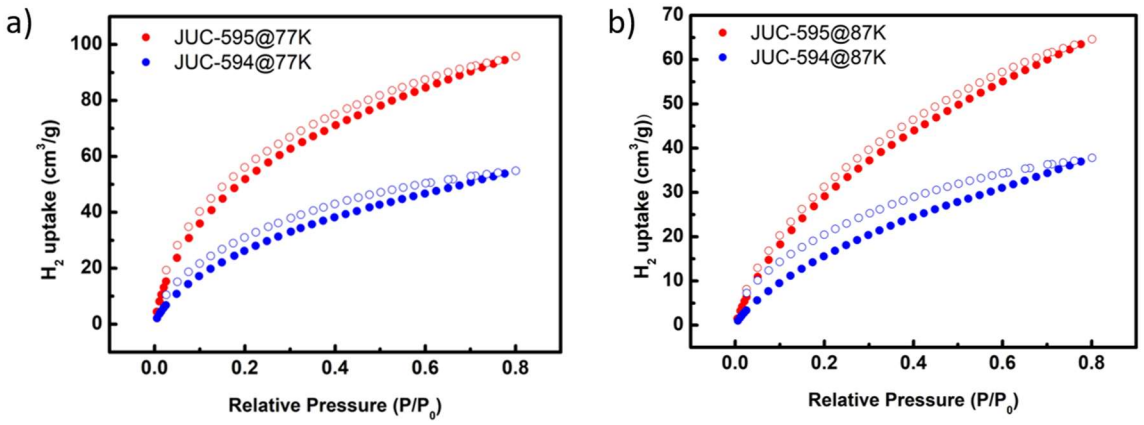

Figure 5. H_2 adsorption isotherms of JUC-594 (a) and JUC-595 (b) at 77 and 78 K.

4. Conclusions

In summary, we used a pre-locked linker as a novel strategy for breaking dynamic behavior in 3D COFs. Compared with flexible BD, benzylideneamine moiety in DPP conformationally-locks the linker and greatly restrict the molecular-bond rotation of imine linkage in JUC-595. This strategy afforded rigid 3D framework even under solvent inclusion and release, while JUC-594 exhibited reversible transformation driven by its flexible imine bonds. Beneficially, improved surface area was seen in JUC-595 compared with JUC-549. Accordingly, JUC-595 recorded an enhanced CO_2, CH_4, and H_2 storage relative to JUC-594. This study serves an important insight on breaking the dynamic behavior in 3D COFs affecting the gas storage performances.

Supplementary Materials: The following supporting information can be downloaded at: Preprints.org, Figure S1-S2: FT-IR spectra; Figure S3-S4: SEM and TEM images; Figure S5-S6: TGA curves; Figure S7-S10: PXRD patterns; Figure S11-S15: Porosity analysis; Figure S16-S17: The H2 Q_{st}; Table S1: H_2 Q_{st} of several reported 3D COFs; Table S2-S2: Unit cell parameters and fractional atomic coordinates.

Author Contributions: X.C. and C.Y. conceptualization, data curation, formal analysis, investigation, methodology, writing—original draft; Y. Y. writing—review and editing, supervision, validation; S. Q. writing—review and editing; Q.F. writing—review and editing, supervision, validation, resources, funding acquisition, project administration. The manuscript was written through the contributions of all authors. All authors have read and agreed to the published version of the manuscript.

Funding: This work was supported by National Key R&D Program of China (2021YFF0500504 and 2022YFB3704900), National Natural Science Foundation of China (22025504, 21621001, and 22105082), the SINOPEC Research Institute of Petroleum Processing, "111" Project (BP0719036 and B17020), and the program for JLU Science and Technology Innovative Research Team. Y.Y. thank to Jilin University "Dingxin Scholar" program for financial support.

Data Availability Statement: Not applicable.

Conflicts of Interest: The authors declare no conflict of interest.

References

1. Coˆté, A.P.; Benin, A.I.; Ockwig, N.W.; O'Keeffe, M.; Matzger, A.J.; Yaghi, O.M. Porous, Crystalline, Covalent Organic Frameworks. *Science* **2005**, *310*, 1166
2. Feng, X.; Ding, X.; Jiang, D. Covalent Organic Frameworks. *Chem. Soc. Rev.* **2012**, *41*, 6010.
3. Ding, S.Y.; Wang, W. Covalent Organic Frameworks (COFs): From Design to Applications. *Chem. Soc. Rev.* **2013**, *42*, 548.
4. Diercks, C.S.; Yaghi, O.M. The Atom, the Molecule, and the Covalent Organic Framework. *Science* **2017**, *355*, eaal1585.
5. Liu, Y.; Ren, J.; Wang, Y.; Zhu, X.; Guan, X.; Wang, Z.; Zhou, Y.; Zhu, L.; Qiu, S.; Xiao, S.; et al. A Stable Luminescent Covalent Organic Framework Nanosheet for Sensitive Molecular Recognition. *CCS Chem.* **2023**, *5*, 2033.

6. Liang, R.R.; Cui, F.Z.; Han, R.; Qi, Q.Y.; Zhao, X. A Study on Constitutional Isomerism in Covalent Organic Frameworks: Controllable Synthesis, Transformation, and Distinct Difference in Properties. *CCS Chem.* **2020**, *2*, 139.
7. He, C.; Wu, Q.J.; Mao, M.J.; Zou, Y.H.; Liu, B.T.; Huang, Y.B.; Cao, R. Multifunctional Gold Nanoparticles@imidazolium-Based Cationic Covalent Triazine Frameworks for Efficient Tandem Reactions. *CCS Chem.* **2021**, *3*, 2368.
8. Wang, Z.; Liu, Y.; Wang, Y.; Fang, Q. A New Covalent Organic Framework Modified with Sulfonic Acid for CO2 Uptake and Selective Dye Adsorption. *Acta Chim. Sin.* **2022**, *80*, 37.
9. Li, M.; Liu, J.; Li, Y.; Xing, G.; Yu, X.; Peng, C.; Chen, L. Skeleton Engineering of Isostructural 2D Covalent Organic Frameworks: Orthoquinone Redox-Active Sites Enhanced Energy Storage. *CCS Chem.* **2021**, *3*, 696.
10. Chang, S.; Li, C.; Li, H.; Zhu, L.; Fang, Q. Stable Thiophene-Sulfur Covalent Organic Frameworks for Oxygen Reduction Reaction(ORR). *Chem. Res. Chinese Univ.* **2022**, *38*, 396.
11. Fu, J.; Liu, J.Y.; Zhang, G.H.; Zhu, Q.H.; Wang, S.L.; Qin, S.; He, L.; Tao, G.H. Boost of Gas Adsorption Kinetics of Covalent Organic Frameworks via Ionic Liquid Solution Process. *Small* **2023**, *19*, 2302570.
12. Wang, H.; Yang, Y.; Yuan, X.; Liang Teo, W.; Wu, Y.; Tang, L.; Zhao, Y. Structure–Performance Correlation Guided Applications of Covalent Organic Frameworks. *Mater. Today* **2022**, *53*, 106.
13. Liu, R.; Tan, K.T.; Gong, Y.; Chen, Y.; Li, Z.; Xie, S.; He, T.; Lu, Z.; Yang, H.; Jiang, D. Covalent Organic Frameworks: An Ideal Platform for Designing Ordered Materials and Advanced Applications. *Chem. Soc. Rev.* **2021**, *50*, 120.
14. Carrington, M.E.; Rampal, N.; Madden, D.G.; O'Nolan, D.; Casati, N.P.M.; Divitini, G.; Martín-Illán, J.; Tricarico, M.; Cepitis, R.; Çamur, C.; et al. Sol-Gel Processing of a Covalent Organic Framework for the Generation of Hierarchically Porous Monolithic Adsorbents. *Chem* **2022**, *8*, 2961.
15. Wang, Z.; Zhang, S.; Chen, Y.; Zhang, Z.; Ma, S. Covalent Organic Frameworks for Separation Applications. *Chem. Soc. Rev.* **2020**, *49*, 708.
16. Li, Y.; Sui, J.; Cui, L.S.; Jiang, H.L. Hydrogen Bonding Regulated Flexibility and Disorder in Hydrazone-Linked Covalent Organic Frameworks. *J. Am. Chem. Soc.* **2023**, *145*, 1359.
17. Ma, Y.X.; Li, Z.J.; Wei, L.; Ding, S.Y.; Zhang, Y.B.; Wang, W. A Dynamic Three-Dimensional Covalent Organic Framework. *J. Am. Chem. Soc.* **2017**, *139*, 4995.
18. Zhu, Q.; Wang, X.; Clowes, R.; Cui, P.; Chen, L.; Little, M.A.; Cooper, A.I. 3D Cage Cofs: A Dynamic Three-Dimensional Covalent Organic Framework with High-Connectivity Organic Cage Nodes. *J. Am. Chem. Soc.* **2020**, *142*, 16842.
19. Wu, X.; Han, X.; Liu, Y.; Liu, Y.; Cui, Y. Control Interlayer Stacking and Chemical Stability of Two-Dimensional Covalent Organic Frameworks via Steric Tuning. *J. Am. Chem. Soc.* **2018**, *140*, 16124.
20. Chen, X.; Addicoat, M.; Irle, S.; Nagai, A.; Jiang, D. Control of Crystallinity and Porosity of Covalent Organic Frameworks by Managing Interlayer Interactions Based on Self-Complementary π-Electronic Force. *J. Am. Chem. Soc.* **2013**, *135*, 546.
21. Wang, Y.; Liu, Y.; Li, H.; Guan, X.; Xue, M.; Yan, Y.; Valtchev, V.; Qiu, S.; Fang, Q. Three-Dimensional Mesoporous Covalent Organic Frameworks through Steric Hindrance Engineering. *J. Am. Chem. Soc.* **2020**, *142*, 3736.
22. Zhang, Y.; Li, H.; Chang, J.; Guan, X.; Tang, L.; Fang, Q.; Valtchev, V.; Yan, Y.; Qiu, S. 3D Thioether-Based Covalent Organic Frameworks for Selective and Efficient Mercury Removal. *Small* **2021**, *17*, 2006112.
23. Xu, Y.; Sun, T.; Zeng, T.; Zhang, X.; Yao, X.; Liu, S.; Shi, Z.; Wen, W.; Zhao, Y.; Jiang, S.; et al. Symmetry-Breaking Dynamics in a Tautomeric 3D Covalent Organic Framework. *Nat. Commun.* **2023**, *14*, *4215.*
24. Wu, Z.; Wei, W.; Ma, J.; Luo, J.; Zhou, Y.; Zhou, Z.; Liu, S. Adsorption of Iodine on Adamantane-Based Covalent Organic Frameworks. *ChemistrySelect* **2021**, *6*, 10141.
25. Zhang, Y.-B.; Su, J.; Furukawa, H.; Yun, Y.; Gándara, F.; Duong, A.; Zou, X.; Yaghi, O.M. Single-Crystal Structure of a Covalent Organic Framework. *J. Am. Chem. Soc.* **2013**, *135*, 16336.
26. Materials Studio ver. 7.0; Accelrys Inc.: San Diego, CA, 2013.
27. Krause, S.; Hosono, N.; Kitagawa, S. Chemistry of Soft Porous Crystals: Structural Dynamics and Gas Adsorption Properties. *Angew. Chem. Int. Ed.* **2020**, *59*, 15325.
28. Liu, X.; Li, J.; Gui, B.; Lin, G.; Fu, Q.; Yin, S.; Liu, X.; Sun, J.; Wang, C. A Crystalline Three-Dimensional Covalent Organic Framework with Flexible Building Blocks. *J. Am. Chem. Soc.* **2021**, *143*, 2123.
29. Chen, Y.; Shi, Z.L.; Wei, L.; Zhou, B.; Tan, J.; Zhou, H.L.; Zhang, Y.B. Guest-Dependent Dynamics in a 3D Covalent Organic Framework. *J. Am. Chem. Soc.* **2019**, *141*, 3298.
30. Mueller-Langer, F.; Tzimas, E.; Kaltschmitt, M.; Peteves, S. Techno-Economic Assessment of Hydrogen Production Processes for the Hydrogen Economy for the Short and Medium Term. *Int. J. Hydrogen Energy* **2007**, *32*, 3797.
31. Furukawa, H.; Yaghi, O.M. Storage of Hydrogen, Methane, and Carbon Dioxide in Highly Porous Covalent Organic Frameworks for Clean Energy Applications. *J. Am. Chem. Soc.* **2009**, *131*, 8875.

32. Yu, C.; Li, H.; Wang, Y.; Suo, J.; Guan, X.; Wang, R.; Valtchev, V.; Yan, Y.; Qiu, S.; Fang, Q. Three-Dimensional Triptycene-Functionalized Covalent Organic Frameworks with Hea Net for Hydrogen Adsorption. *Angew. Chem. Int. Ed.* **2022**, *61, e202117101.*
33. Li, H.; Chen, F.; Guan, X.; Li, J.; Li, C.; Tang, B.; Valtchev, V.; Yan, Y.; Qiu, S.; Fang, Q. Three-Dimensional Triptycene-Based Covalent Organic Frameworks with Ceq or Acs Topology. *J. Am. Chem. Soc.* **2021**, *143*, 2654.